IEEE Photonics Journal
An IEEE Photonics Society Publication

Open Access

An Efficient Numerical Full-Vectorial Mode Solver Based on Fourier Series Expansion Method

Volume 6, Number 4, August 2014

C. S. Hsiao
Y. J. Chiang
Likarn Wang
T. K. Ching

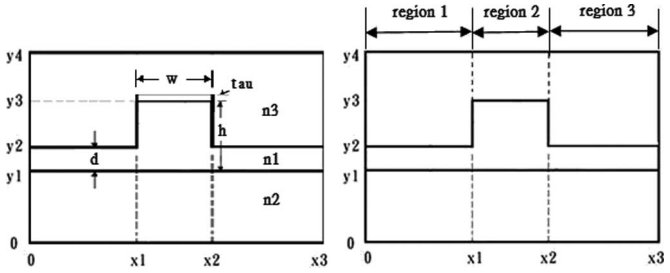

DOI: 10.1109/JPHOT.2014.2335714
1943-0655 © 2014 IEEE

IEEE photonics SOCIETY

IEEE

An Efficient Numerical Full-Vectorial Mode Solver Based on Fourier Series Expansion Method

C. S. Hsiao,[1] Y. J. Chiang,[2] Likarn Wang,[3] and T. K. Ching[4]

[1]Department of Photonics and Communications, Asia University, Taichung 41354, Taiwan
[2]Department of Electronic Engineering, Oriental Institute of Technology, Taipei 220, Taiwan
[3]Institute of Photonics Technologies, National Tsing Hua University, Hsinchu 30013, Taiwan
[4]Department of Electrical Engineering, National Chi Nan University, Nantou 54561, Taiwan

DOI: 10.1109/JPHOT.2014.2335714

Manuscript received January 22, 2014; accepted June 27, 2014. Date of publication July 8, 2014; date of current version July 28, 2014. This work was supported in part by Asia University under Grant 100-a-28 and Grant 102-asia-46; by NSC, Taiwan, under Grant 101-2221-E-468-014 and Grant 102-2221-E-007-089; and by National Tsing Hua University under Grant 102N2080E1. Corresponding author: L. Wang (e-mail: lkwang@ee.nthu.edu.tw).

Abstract: A new algorithm of full-vectorial eigenmode solver is presented, which is utilized to determine the modal index of dielectric optical waveguides. The approach is based on the Fourier cosine and sine series expansions of the magnetic field distributions and the refractive index profile. By substituting these series expansions in the wave equation, a pair of second-order differential matrix equations is obtained by collecting all the terms with the same spatial frequency. With boundary conditions used, a matrix equation with a dimension of $(N+1)$ by $(N+1)$, where N is the number of terms for truncated series, is obtained, which can be easily solved by using the Newton–Raphson root-shooting algorithm. The presented scheme requires considerably less computational time and memory storage by only considering the finite terms of the Fourier cosine/sinusoidal series. Calculated results by our proposed method are in good agreement with those obtained by BeamPROP and COMSOL and compare well with other available methods, demonstrating the accuracy and efficiency and also the applicability of our proposed method.

Index Terms: Full-vectorial eigenmode, differential matrix equations, Newton–Raphson root-shooting algorithm.

1. Introduction

Optical waveguides play a key role in photonic devices used in optical communication systems such as modulators, polarizers, beam splitters, wavelength-division multiplexing components, etc. Modal analysis of an optical waveguide is an important issue for understanding the wave characteristics through investigation of the propagation constant and the field distribution. Up to now, many numerical approaches have been proposed to study the optical characteristics of 3-D dielectric optical waveguides and photonic crystals. Among those, the finite difference method (FDM) [1]–[7] has advantages of holding simple formulation and can lead to accurate results but at the expense of CPU time and memory storage required. The finite element method (FEM) [8]–[12] has merit of providing more accurate modal parameters near cutoff condition while having the disadvantage of requiring large storage memory and CPU time. The

series expansion method (SEM) [13]–[17] is considered as a powerful method for eigenmode solution because of less requirement for computer memory when it is used to solve simple waveguide problems, as compared with FDM and FEM, while it is prone to oscillation of modal index and henceforth resulting in poor convergence for waveguides with discontinuous refractive index profile at boundaries. The pseudospectral domain scheme [18]–[20] has been proposed recently to compute the modal index by dividing the calculated domain into several subdomains. Subdomains are then connected with conditions of electromagnetic field being continuous at dielectric interfaces. The wave equation is expanded by the orthogonal basis Laguerre–Gauss functions and Chebyshev polynomials to form the eigenvalue matrix equation and thus solved by power inverse scheme. This approach seems to have a problem of requiring large memory and CPU time. The vector beam propagation method (VBPM) [21] is a split-operator method of combining the FFT, Pade' approximation with the alternating direction implicit (ADI) method, which has the operators of phase adjustment, polarization rotation, homogeneous propagation, and cross coupling to be decomposed and multiplied to avoid inversion of the cross-coupling terms existing in the full-vectorial equation, while being prone to large CPU time, instability, and convergence problems. Additionally, the noniterative full-vectorial beam propagation with ADI method longitudinally discretizes the waveguide structure by means of the Crank–Nicholson scheme. Therefore, this approach keeps advantage of shortening computation time, while it seems to be not able to attain higher accuracy. The variational method [22] based on the scalar variational principle plus vector perturbation analysis and a trial function was proposed to analyze the propagation constant of optical waveguide. Other methods were developed and presented in the past years to study dielectric rib waveguide [23]–[25]. Recently, an effective scalar beam propagation method has been proposed by expanding the field and the refractive index distribution into Fourier series in azimuthal direction to gain speed advantage [26].

In this paper, we propose a Fourier series expansion method to study for the first time the full vectorial modes of dielectric waveguides by treating less matrix calculation formed by this approach. We expand the magnetic field distributions and the refractive index profile into the Fourier cosine and sine series and substitute these series in the wave equation. Subsequently a matrix equation can be derived by using boundary conditions. Numerical results could be readily obtained by Newton–Raphson root-shooting algorithm applied in solving this matrix equation. Although the concept of Fourier series expansion was also used by [26] in the azimuthal direction of a cylindrical coordinate system, the proposed method does not use a finite difference treatment as [26] did to form a matrix equation. Instead, we divide the transverse domain of the concerned waveguide into three subdomains, treat the wave equation by Fourier series expansion in each subdomain, and then obtain analytical solutions for the fields of all three domains. The two-dimensional problem is thus transformed to a one-dimensional problem, in which only one-dimensional Fourier series expansion is required. An eigenvalue problem with a matrix for obtaining mode indices is thus of dimension N, where N is the number of Fourier series terms. Consequently, in solving for eigenmodes, this method is more efficient than that using 2-D Fourier series expansion [27]–[29], in the latter of which a matrix of dimension $N \times M$ (with double series expansions) is required, with N and M being the numbers of Fourier series terms for x and y dimensions, respectively. On the other hand, the presented method here is also believed to be more efficient in computation than FDM or FEM, which requires a large grid number in many cases.

The content of this paper is organized as follows. The derivation of the matrix equation for the calculation of the modal index of dielectric optical waveguides is described in Section 2. In Section 3, examples of rib waveguides are taken in our proposed method. The numerical results obtained using the proposed method are then compared with those obtained by the commercial software BeamPROP and the multiphysics package COMSOL, which is an electromagnetic full-wave beam propagation method for overcoming the traditional approximation problem by elastical discretization of the studied waveguide structure, as well as those by other numerical methods. Finally, this paper is concluded in Section 4.

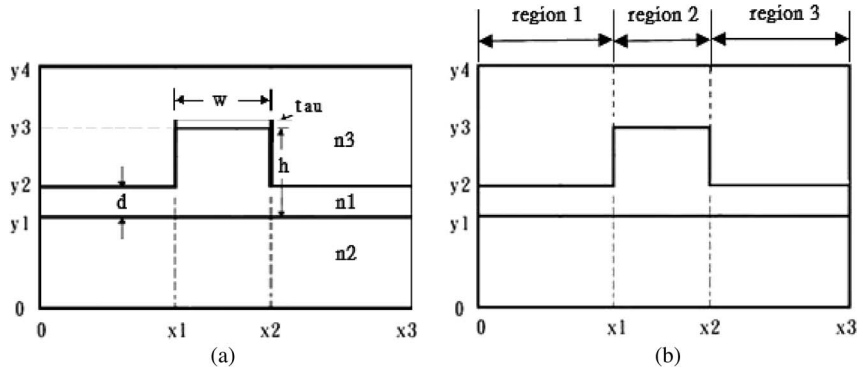

Fig. 1. Cross-sectional structure of the optical waveguide under study. (a) Structural parameters, where n_1, n_2, and n_3 are the refractive indices of the guiding layer, the substrate region, and the cover region, respectively; h and w are the height and width of the rib region, respectively; and d is the slab's thickness. In (b), the cross section is divided into three regions. In the study, the rib may also be covered by a gold film with a thickness of t_{au}.

2. Formulation of the Proposed Method

Fig. 1(a) shows the geometric structure of dielectric waveguide under study. In Fig. 1(b), the cross section of the waveguide is divided into three regions, i.e., regions 1, 2, and 3. Formulation for the magnetic fields is derived here because the electric fields appear discontinuous at some interfaces while magnetic fields are continuous everywhere. The derivation of the mode solver starts with the source free full-vectorial magnetic field wave equations given by

$$\frac{\partial^2 H_x^i}{\partial x^2} + \varepsilon_{ri}\frac{\partial}{\partial y}\left(\frac{1}{\varepsilon_{ri}}\frac{\partial H_x^i}{\partial y}\right) + \left(k_0^2\varepsilon_{ri}(x,y) - \beta^2\right)H_x^i + \frac{1}{\varepsilon_{ri}}\frac{\partial \varepsilon_{ri}}{\partial y}\frac{\partial H_y^i}{\partial x} = 0 \tag{1}$$

and

$$\frac{\partial^2 H_y^i}{\partial y^2} + \varepsilon_{ri}\frac{\partial}{\partial x}\left(\frac{1}{\varepsilon_{ri}}\frac{\partial H_y^i}{\partial x}\right) + \left(k_0^2\varepsilon_{ri}(x,y) - \beta^2\right)H_y^i + \frac{1}{\varepsilon_{ri}}\frac{\partial \varepsilon_{ri}}{\partial x}\frac{\partial H_x^i}{\partial y} = 0 \tag{2}$$

where $k_0 = 2\pi/\lambda$ is the wavenumber in free space; ε_r $(i = 1, 2,$ and $3)$ stands for relative permittivity at the corresponding region as shown in Fig. 1(b); λ is the wavelength in vacuum; and $\beta = n_{eff}\, k_0$ is the propagation constant with n_{eff} being the mode index to be determined. Here, H_x^i and H_y^i represent the transverse magnetic field components in region i. To solve (1) and (2) for different regions, the parameters ε_r and the transverse magnetic field H_x^i and H_y^i are expanded into Fourier cosine and sine series as follows:

$$\left(\varepsilon_{ri}, H_x^1, H_y^1\right) = \left(\sum_{n=0}^{N} a_n \cos n\Delta\omega y, \sum_{n=0}^{N} h_{xn}^1 \cos n\Delta\omega y, \sum_{n=1}^{N+1} h_{yn}^1 \sin n\Delta\omega y\right) \quad \text{for region 1}$$

$$\left(\varepsilon_{ri}, H_x^2, H_y^2\right) = \left(\sum_{n=0}^{N} b_n \cos n\Delta\omega y, \sum_{n=0}^{N} h_{xn}^2 \cos n\Delta\omega y, \sum_{n=1}^{N+1} h_{yn}^2 \sin n\Delta\omega y\right) \quad \text{for region 2}$$

$$\left(\varepsilon_{ri}, H_x^3, H_y^3\right) = \left(\sum_{n=0}^{N} c_n \cos n\Delta\omega y, \sum_{n=0}^{N} h_{xn}^3 \cos n\Delta\omega y, \sum_{n=1}^{N+1} h_{yn}^3 \sin n\Delta\omega y\right) \quad \text{for region 3} \tag{3}$$

where $\Delta\omega$ is given by $\Delta\omega = \pi/y_4$, and N stands the number of the Fourier series terms with large value for numerical convergence. In addition, φ_x^i and φ_y^i $(i = 1, 2, \text{ and } 3)$ are defined as

$$\begin{aligned}
\varphi_x^1 &= \frac{1}{\varepsilon_{r1}}\frac{\partial H_x^1}{\partial y} = \sum_{n=1}^{N+1}\phi_{xn}^1 \sin n\Delta\omega y, \quad \text{for region 1} \\
\varphi_x^2 &= \frac{1}{\varepsilon_{r2}}\frac{\partial H_x^2}{\partial y} = \sum_{n=1}^{N+1}\phi_{xn}^2 \sin n\Delta\omega y, \quad \text{for region 2} \\
\varphi_x^3 &= \frac{1}{\varepsilon_{r3}}\frac{\partial H_x^3}{\partial y} = \sum_{n=1}^{N+1}\phi_{xn}^3 \sin n\Delta\omega y, \quad \text{for region 3}
\end{aligned} \tag{4}$$

and

$$\begin{aligned}
\varphi_y^1 &= \frac{1}{\varepsilon_{r1}}\frac{\partial H_y^1}{\partial x} = \sum_{n=1}^{N+1}\phi_{yn}^1 \sin n\Delta\omega y, \quad \text{for region 1} \\
\varphi_y^2 &= \frac{1}{\varepsilon_{r2}}\frac{\partial H_y^2}{\partial x} = \sum_{n=1}^{N+1}\phi_{yn}^2 \sin n\Delta\omega y, \quad \text{for region 2} \\
\varphi_y^3 &= \frac{1}{\varepsilon_{r3}}\frac{\partial H_y^3}{\partial x} = \sum_{n=1}^{N+1}\phi_{yn}^3 \sin n\Delta\omega y, \quad \text{for region 3}
\end{aligned} \tag{5}$$

Note that we here expanded the y component of the magnetic field by the Fourier sine series and then substituted it into (1) and (2) to form a whole Fourier cosine series listed in (6). Note that the superscripts 1, 2, and 3 in the expressions above for transverse magnetic field components of Fourier series expansion denote different regions. Also note that we have extended the cross-section of the analyzed region such that one period in the x direction is from $-x_3$ to x_3 and that in the y direction one period is from $-y_4$ and y_4 for the sake of generality. Substitution of the definitions for region 1 in (3)–(5) into (1) leads to

$$\begin{aligned}
&\sum_{n=0}^{N}\frac{\partial^2 h_x^1}{\partial x^2}\cos n\Delta\omega y + \frac{1}{2}\sum_{m=0}^{N}\sum_{n=1}^{N+1} a_m(n\Delta\omega)\phi_{xn}^1[\cos(m+n)\Delta\omega y + \cos(m-n)\Delta\omega y] \\
&\quad + \frac{1}{2}k_0^2\sum_{m=0}^{N}\sum_{n=0}^{N} a_m h_{xn}^1[\cos(m+n)\Delta\omega y + \cos(m-n)\Delta\omega y] - \beta^2\sum_{m=0}^{N} h_{xn}^1\cos n\Delta\omega y \\
&\quad + \frac{1}{2}\sum_{m=0}^{N}\sum_{n=1}^{N+1} a_m(m\Delta\omega)\phi_{yn}^1[\cos(m+n)\Delta\omega y + \cos(m-n)\Delta\omega y] = 0.
\end{aligned} \tag{6}$$

By equating the coefficient of every spatial frequency component in (6) to zero, we obtain $N+1$ second-order differential equations for region 1, which can be written as follows:

$$\frac{\partial^2}{\partial x^2}\begin{bmatrix} {h_{x_0}}^1 \\ {h_{x_1}}^1 \\ {h_{x_2}}^1 \\ . \\ . \\ . \\ {h_{x_N}}^1 \end{bmatrix} + \frac{1}{2}A_1\begin{bmatrix} {\phi_{x_1}}^1 \\ {\phi_{x_2}}^1 \\ {\phi_{x_3}}^1 \\ . \\ . \\ . \\ {\phi_{x_{N+1}}}^1 \end{bmatrix} + \frac{1}{2}k_0^2 B_1\begin{bmatrix} {h_{x_0}}^1 \\ {h_{x_1}}^1 \\ {h_{x_2}}^1 \\ . \\ . \\ . \\ {h_{x_N}}^1 \end{bmatrix} - \beta^2 I\begin{bmatrix} {h_{x_0}}^1 \\ {h_{x_1}}^1 \\ {h_{x_2}}^1 \\ . \\ . \\ . \\ {h_{x_N}}^1 \end{bmatrix} + \frac{1}{2}C_1\begin{bmatrix} {\phi_{y_1}}^1 \\ {\phi_{y_2}}^1 \\ {\phi_{y_3}}^1 \\ . \\ . \\ . \\ {\phi_{y_{N+1}}}^1 \end{bmatrix} = 0 \quad \text{for region 1.} \tag{7}$$

Similarly, for regions 2 and 3, we can have

$$\frac{\partial^2}{\partial x^2}\begin{bmatrix} {h_{x_0}}^2 \\ {h_{x_1}}^2 \\ {h_{x_2}}^2 \\ \cdot \\ \cdot \\ \cdot \\ {h_{x_N}}^2 \end{bmatrix} + \frac{1}{2}A_2\begin{bmatrix} {\phi_{x_1}}^2 \\ {\phi_{x_2}}^2 \\ {\phi_{x_3}}^2 \\ \cdot \\ \cdot \\ \cdot \\ {\phi_{x_{N+1}}}^2 \end{bmatrix} + \frac{1}{2}k_0^2 B_2\begin{bmatrix} {h_{x_0}}^2 \\ {h_{x_1}}^2 \\ {h_{x_2}}^2 \\ \cdot \\ \cdot \\ \cdot \\ {h_{x_N}}^2 \end{bmatrix} - \beta^2 I\begin{bmatrix} {h_{x_0}}^2 \\ {h_{x_1}}^2 \\ {h_{x_2}}^2 \\ \cdot \\ \cdot \\ \cdot \\ {h_{x_N}}^2 \end{bmatrix} + \frac{1}{2}C_2\begin{bmatrix} {\phi_{y_1}}^2 \\ {\phi_{y_2}}^2 \\ {\phi_{y_3}}^2 \\ \cdot \\ \cdot \\ \cdot \\ {\phi_{y_{N+1}}}^2 \end{bmatrix} = 0 \quad \text{for region 2} \tag{8}$$

$$\frac{\partial^2}{\partial x^2}\begin{bmatrix} {h_{x_0}}^3 \\ {h_{x_1}}^3 \\ {h_{x_2}}^3 \\ \cdot \\ \cdot \\ \cdot \\ {h_{x_N}}^3 \end{bmatrix} + \frac{1}{2}A_3\begin{bmatrix} {\phi_{x_1}}^3 \\ {\phi_{x_2}}^3 \\ {\phi_{x_3}}^3 \\ \cdot \\ \cdot \\ \cdot \\ {\phi_{x_{N+1}}}^3 \end{bmatrix} + \frac{1}{2}k_0^2 B_3\begin{bmatrix} {h_{x_0}}^3 \\ {h_{x_1}}^3 \\ {h_{x_2}}^3 \\ \cdot \\ \cdot \\ \cdot \\ {h_{x_N}}^3 \end{bmatrix} - \beta^2 I\begin{bmatrix} {h_{x_0}}^3 \\ {h_{x_1}}^3 \\ {h_{x_2}}^3 \\ \cdot \\ \cdot \\ \cdot \\ {h_{x_N}}^3 \end{bmatrix} + \frac{1}{2}C_3\begin{bmatrix} {\phi_{y_1}}^3 \\ {\phi_{y_2}}^3 \\ {\phi_{y_3}}^3 \\ \cdot \\ \cdot \\ \cdot \\ {\phi_{y_{N+1}}}^3 \end{bmatrix} = 0 \quad \text{for region 3} \tag{9}$$

where I is the identity matrix, and A_1, B_1, C_1, A_2, B_2, C_2, A_3, B_3, and C_3 are resultant constant full matrices.

Equations (7) to (9) can be further reduced to the following forms:

$$\frac{\partial^2}{\partial x^2}\begin{bmatrix} {h_{x_0}}^1 \\ {h_{x_1}}^1 \\ {h_{x_2}}^1 \\ \cdot \\ \cdot \\ \cdot \\ {h_{x_N}}^1 \end{bmatrix} + K_1\begin{bmatrix} {h_{x_0}}^1 \\ {h_{x_1}}^1 \\ {h_{x_2}}^1 \\ \cdot \\ \cdot \\ \cdot \\ {h_{x_N}}^1 \end{bmatrix} + \frac{1}{2}C_1P_1^{-1}\frac{\partial}{\partial x}\begin{bmatrix} {h_{y_1}}^1 \\ {h_{y_2}}^1 \\ {h_{y_3}}^1 \\ \cdot \\ \cdot \\ \cdot \\ {h_{y_{N+1}}}^1 \end{bmatrix} = 0 \quad \text{for region 1} \tag{10}$$

$$\frac{\partial^2}{\partial x^2}\begin{bmatrix} {h_{x_0}}^2 \\ {h_{x_1}}^2 \\ {h_{x_2}}^2 \\ \cdot \\ \cdot \\ \cdot \\ {h_{x_N}}^2 \end{bmatrix} + K_2\begin{bmatrix} {h_{x_0}}^2 \\ {h_{x_1}}^2 \\ {h_{x_2}}^2 \\ \cdot \\ \cdot \\ \cdot \\ {h_{x_N}}^2 \end{bmatrix} + \frac{1}{2}C_2P_2^{-1}\frac{\partial}{\partial x}\begin{bmatrix} {h_{y_1}}^2 \\ {h_{y_2}}^2 \\ {h_{y_3}}^2 \\ \cdot \\ \cdot \\ \cdot \\ {h_{y_{N+1}}}^2 \end{bmatrix} = 0 \quad \text{for region 2} \tag{11}$$

$$\frac{\partial^2}{\partial x^2}\begin{bmatrix} {h_{x_0}}^3 \\ {h_{x_1}}^3 \\ {h_{x_2}}^3 \\ \cdot \\ \cdot \\ \cdot \\ {h_{x_N}}^3 \end{bmatrix} + K_3\begin{bmatrix} {h_{x_0}}^3 \\ {h_{x_1}}^3 \\ {h_{x_2}}^3 \\ \cdot \\ \cdot \\ \cdot \\ {h_{x_N}}^3 \end{bmatrix} + \frac{1}{2}C_3P_3^{-1}\frac{\partial}{\partial x}\begin{bmatrix} {h_{y_1}}^3 \\ {h_{y_2}}^3 \\ {h_{y_3}}^3 \\ \cdot \\ \cdot \\ \cdot \\ {h_{y_{N+1}}}^3 \end{bmatrix} = 0 \quad \text{for region 3} \tag{12}$$

where the matrices K_1, K_2, and K_3 are defined by $K_1 = (k_0^2/2)B_1 - 1/2A_1P_1^{-1}W - \beta^2 I$, $K_2 = (k_0^2/2)B_2 - 1/2A_2P_2^{-1}W - \beta^2 I$, and $K_3 = (k_0^2/2)B_3 - 1/2A_3P_3^{-1}W - \beta^2 I$. Here P_1, P_2, P_3 are constant full matrices and W is a diagonal matrix.

Next, by substituting the Fourier cosine and sine series expansion of H_y^i, φ_x^i, and φ_y^i into (2), we have the following three differential matrix equations for regions 1, 2, and 3, respectively:

$$\frac{\partial^2}{\partial x^2}\begin{bmatrix} {h_{y_1}}^1 \\ {h_{y_2}}^1 \\ {h_{y_3}}^1 \\ \cdot \\ \cdot \\ \cdot \\ {h_{y_{N+1}}}^1 \end{bmatrix} + S_1 \begin{bmatrix} {h_{y_1}}^1 \\ {h_{y_2}}^1 \\ {h_{y_3}}^1 \\ \cdot \\ \cdot \\ \cdot \\ {h_{y_{N+1}}}^1 \end{bmatrix} = 0 \quad \text{for region 1} \tag{13}$$

$$\frac{\partial^2}{\partial x^2}\begin{bmatrix} {h_{y_1}}^2 \\ {h_{y_2}}^2 \\ {h_{y_3}}^2 \\ \cdot \\ \cdot \\ \cdot \\ {h_{y_{N+1}}}^2 \end{bmatrix} + S_2 \begin{bmatrix} {h_{y_1}}^2 \\ {h_{y_2}}^2 \\ {h_{y_3}}^2 \\ \cdot \\ \cdot \\ \cdot \\ {h_{y_{N+1}}}^2 \end{bmatrix} = 0 \quad \text{for region 2} \tag{14}$$

$$\frac{\partial^2}{\partial x^2}\begin{bmatrix} {h_{y_1}}^3 \\ {h_{y_2}}^3 \\ {h_{y_3}}^3 \\ \cdot \\ \cdot \\ \cdot \\ {h_{y_{N+1}}}^3 \end{bmatrix} + S_3 \begin{bmatrix} {h_{y_1}}^3 \\ {h_{y_2}}^3 \\ {h_{y_3}}^3 \\ \cdot \\ \cdot \\ \cdot \\ {h_{y_{N+1}}}^3 \end{bmatrix} = 0 \quad \text{for region 3} \tag{15}$$

where S_1, S_2, and S_3 are defined by $S_i = (k_0^2/2 \times P_{i-}\overline{W} - \beta^2 I)$, $i = 1, 2,$ and 3. Here $\overline{W}$ is a diagonal matrix.

Explicit solutions to (13)–(15) have the forms, respectively, expressed as

$$\mathbf{H_y^1}(\mathbf{x}) = \sum_{n=0}^{N} H_n \overline{a_n} \exp\left(\sqrt{\beta_n^2 - \kappa_n}(x - x_1)\right) \quad \text{for region 1} \tag{16}$$

$$\mathbf{H_y^2}(\mathbf{x}) = \sum_{n=0}^{N} U_n \overline{f_n} \cos\left(\sqrt{\lambda_n - \beta_n^2}(x - x_1) - \theta_n\right) \quad \text{for region 2} \tag{17}$$

$$\mathbf{H_y^3}(\mathbf{x}) = \sum_{n=0}^{N} W_n \overline{d_n} \exp\left(-\sqrt{\beta_n^2 - \delta_n}(x - x_2)\right) \quad \text{for region 3.} \tag{18}$$

Here $\mathbf{H_y^i}(\mathbf{x})$ are column vectors defined as $[h_{y1}^i, h_{y2}^i, \ldots h_{yN+1}^i]^T$, $i = 1,\ 2,$ and 3 with T denoting a transpose. Parameters $\kappa_n(H_n)$, $\lambda_n(U_n)$, and $\delta_n(W_n)$ $(n = 0, 1, 2, \ldots\ldots, N)$ are the nth eigenvalues (eigenvectors) of $(k_0^2/2 \times P_1 - \overline{W})$, $(k_0^2/2 \times P_2 - \overline{W})$, and $(k_0^2/2 \times P_{3-}\overline{W})$, respectively. It should be noted that $\overline{a_n} = \overline{d_n}$, $H_n = W_n$, and $\kappa_n = \delta_n$ hold for the waveguide structure shown in Fig. 1 because of symmetry of the waveguide structure. $\overline{a_n}$, $\overline{f_n}$, θ_n, and $\overline{d_n}$ $(n = 0, 1, 2, \ldots, N)$ are numbers. The parameters$\overline{f_n}$ and θ_n are to be determined from the boundary conditions. Once $\overline{f_n}$ and θ_n are solved, $\mathbf{H_y^i}(\mathbf{x})$ and henceforth the magnetic field can be found.

The homogeneous solutions to (10)–(12) are given as

$$\mathbf{H_{xh}^1}(\mathbf{x}) = \sum_{n=0}^{N} Q_n \overline{b_n} \exp\left(\sqrt{\beta^2 - \alpha_n}(x - x_1)\right) \quad \text{for region 1} \tag{19}$$

$$\mathbf{H}^2_{\mathbf{xh}}(\mathbf{x}) = \sum_{n=0}^{N} R_n \overline{g_n} \cos\left(\sqrt{\gamma_n - \beta^2}(x - x_1) - \phi_n\right) \quad \text{for region 2} \tag{20}$$

$$\mathbf{H}^3_{\mathbf{xh}}(\mathbf{x}) = \sum_{n=0}^{N} T_n \overline{m_n} \exp\left(-\sqrt{\beta^2 - \sigma_n}(x - x_2)\right) \quad \text{for region 3} \tag{21}$$

where $\alpha_n(Q_n)$, $\gamma_n(R_n)$, and $\sigma_n(T_n)$ $(n = 0, 1, \ldots, N)$ are the nth eigenvalues (eigenvectors) of $[(k_0^2/2)B_1 - 1/2A_1P_1^{-1}W]$, $[(k_0^2/2)B_2 - 1/2A_2P_2^{-1}W]$, and $[(k_0^2/2)B_3 - 1/2A_3P_3^{-1}W]$, respectively. The parameters $\overline{b_n}$, $\overline{g_n}$, and $\overline{m_n}$ are numbers to be determined. It should be noted that $\overline{b_n} = \overline{m_n}$, $Q_n = T_n$, and $\alpha_n = \sigma_n$ are valid because of symmetry of the waveguide structure.

The particular solutions to (10)–(12) are given as follows:

$$\mathbf{H}^1_{\mathbf{xp}}(\mathbf{x}) = \sum_{n=0}^{N} H_n \sqrt{\beta^2 - \kappa_n} \overline{c_n} \exp\left(\sqrt{\beta^2 - \kappa_n}(x - x_1)\right) \quad \text{for region 1} \tag{22}$$

$$\mathbf{H}^2_{\mathbf{xp}}(\mathbf{x}) = -\sum_{n=0}^{N} U_n \sqrt{\lambda_n - \beta^2} \overline{h_n} \sin\left(\sqrt{\lambda_n - \beta^2}(x - x_1) - \theta_n\right) \quad \text{for region 2} \tag{23}$$

$$\mathbf{H}^3_{\mathbf{xp}}(\mathbf{x}) = -\sum_{n=0}^{N} W_n \sqrt{\beta^2 - \delta_n} \overline{j_n} \exp\left(-\sqrt{\beta_n^2 - \delta_n}(x - x_2)\right) \quad \text{for region 3.} \tag{24}$$

Here, note that $\overline{c_n}$, $\overline{h_n}$, and $\overline{j_n}$ $(n = 0, 1, 2, \ldots, N)$ are also numbers. Similarly, $\overline{c_n} = \overline{j_n}$ hold for the symmetry of the waveguide structure.

Therefore, the complete solutions for magnetic components in the x direction are expressed as

$$\mathbf{H}^1_{\mathbf{xc}}(\mathbf{x}) = \sum_{n=0}^{N} Q_n \overline{b_n} \exp\left(\sqrt{\beta^2 - \alpha_n}(x - x_1)\right) + \sum_{n=0}^{N} H_n \sqrt{\beta^2 - \kappa_n} \overline{c_n} \exp\left(\sqrt{\beta^2 - \kappa_n}(x - x_1)\right) \tag{25}$$

$$\mathbf{H}^2_{\mathbf{xc}}(\mathbf{x})1 = \sum_{n=0}^{N} R_n \overline{g_n} \cos\left(\sqrt{\gamma_n - \beta^2}(x - x_1) - \phi_n\right) - \sum_{n=0}^{N} U_n \sqrt{\lambda_n - \beta^2} \overline{h_n} \sin\left(\sqrt{\lambda_n - \beta^2}(x - x_1) - \theta_n\right) \tag{26}$$

$$\mathbf{H}^3_{\mathbf{xc}}(\mathbf{x}) = \sum_{n=0}^{N} T_n \overline{m_n} \exp\left(-\sqrt{\beta^2 - \sigma_n}(x - x_2)\right) - \sum_{n=0}^{N} W_n \sqrt{\beta^2 - \delta_n} \overline{j_n} \exp\left(-\sqrt{\beta_n^2 - \delta_n}(x - x_2)\right). \tag{27}$$

The parameters ψ_n, $\overline{b_n}$, $\overline{c_n}$, $\overline{g_n}$, $\overline{h_n}$, $\overline{j_n}$, and $\overline{m_n}$ $(n = 0, 1, 2, \ldots, N)$ are to be determined from the boundary conditions of the magnetic and electric fields at the interfaces.

The continuities of the magnetic field components at $x = x_1$ and $x = x_2$ require

$$\mathbf{H}^1_{\mathbf{xc}}(\mathbf{x_1}) = \mathbf{H}^2_{\mathbf{xc}}(\mathbf{x_1}) \tag{28}$$

$$\mathbf{H}^1_{\mathbf{y}}(\mathbf{x_1}) = \mathbf{H}^2_{\mathbf{y}}(\mathbf{x_1}) \tag{29}$$

$$\mathbf{H}^2_{\mathbf{xc}}(\mathbf{x_2}) = \mathbf{H}^3_{\mathbf{xc}}(\mathbf{x_2}) \tag{30}$$

$$\mathbf{H}^2_{\mathbf{y}}(\mathbf{x_2}) = \mathbf{H}^3_{\mathbf{y}}(\mathbf{x_2}) \tag{31}$$

$$\mathbf{H}^1_{\mathbf{z}}(\mathbf{x_1}) = \mathbf{H}^2_{\mathbf{z}}(\mathbf{x_1}) \tag{32}$$

$$\mathbf{H}^2_{\mathbf{z}}(\mathbf{x_2}) = \mathbf{H}^3_{\mathbf{z}}(\mathbf{x_2}). \tag{33}$$

Here, the z-component of magnetic field vector $\mathbf{H}^{\mathbf{i}}_{\mathbf{z}}$ $(i = 1, 2, \text{ and } 3)$ are related to $\mathbf{H}^{\mathbf{i}}_{\mathbf{x}}$ and $\mathbf{H}^{\mathbf{i}}_{\mathbf{y}}$ in accordance with the divergence theorem of the magnetic field $\nabla \cdot H = 0$. Equations (28)–(33) lead to the following matrix equations:

$$Q\overline{\overline{b}} + HM_2(\beta)\overline{\overline{c}} = R\overline{\overline{g_c}} + UM_4(\beta)\overline{\overline{h_s}} \tag{34}$$

$$H\overline{\overline{a}} = U\overline{\overline{f_c}} \tag{35}$$

$$R\left(Y_{rc}(\beta)\overline{\overline{g_c}}+Y_{rs}(\beta)\overline{\overline{g_s}}\right)-UM_4(\beta)\left(Y_s(\beta)\overline{\overline{h_c}}+Y_c(\beta)\overline{\overline{h_s}}\right)=T\overline{\overline{m_n}}+\overline{\overline{W}}M_2(\beta)\overline{\overline{c}} \tag{36}$$

$$U\left(Y_c(\beta)\overline{\overline{f_c}}+Y_s(\beta)\overline{\overline{f_s}}\right)=\overline{\overline{Wd}} \tag{37}$$

$$QM_1(\beta)\overline{\overline{b}}+HM_2(\beta)^2\overline{\overline{c}}=RM_3(\beta)\overline{\overline{g_s}}-UM_4(\beta)^2\overline{\overline{h_c}} \tag{38}$$

$$RM_3(\beta)\left(Y_{rs}(\beta)\overline{\overline{g_c}}-Y_{rc}(\beta)\overline{\overline{g_s}}\right)+UM_4(\beta)^2\left(Y_c(\beta)\overline{\overline{h_c}}+Y_s(\beta)\overline{\overline{h_s}}\right)=TM_5(\beta)\overline{\overline{m}}+\overline{\overline{W}}M_6(\beta)^2\overline{\overline{c}} \tag{39}$$

where $\overline{\overline{a}}$, $\overline{\overline{b}}$, $\overline{\overline{c}}$, $\overline{\overline{d}}$, and $\overline{\overline{m}}$ are column vectors given by $\overline{\overline{a}}=[\overline{a_0},\overline{a_1},\ldots,\overline{a_N}]^T$, $\overline{\overline{b}}=[\overline{b_0},\overline{b_1},\ldots,\overline{b_N}]^T$, $\overline{\overline{c}}=[\overline{c_0},\overline{c_1},\ldots,\overline{c_N}]^T$, $\overline{\overline{d}}=[\overline{d_0},\overline{d_1},\ldots,\overline{d_N}]^T$, and $\overline{\overline{m}}=[\overline{m_0},\overline{m_1},\ldots,\overline{m_N}]^T$ with $\overline{\overline{a}}$ being an arbitrary column vector. The column vectors $\overline{\overline{g_c}}$, $\overline{\overline{g_s}}$, $\overline{\overline{f_c}}$, $\overline{\overline{f_s}}$, $\overline{\overline{h_c}}$, and $\overline{\overline{h_s}}$ are defined by $\overline{\overline{g_c}}=[\overline{g_0}\cos\phi_0,\ \overline{g_1}\cos\phi_1,\ldots,\overline{g_N}\ cos\phi_N]^T$, $\overline{\overline{g_s}}=[\overline{g_0}\sin\phi_0,\overline{g_1}\sin\phi_1,\ldots,\overline{g_N}\ sin\phi_N]^T$, $\overline{\overline{f_c}}=[\overline{f_0}\cos\phi_0,\overline{f_1}\cos\phi_1,\ldots,\ \overline{f_N}\ cos\phi_N]^T$, $\overline{\overline{f_s}}=[\overline{f_0}\sin\phi_0,\overline{f_1}\sin\phi_1,\ldots,\overline{f_N}\ sin\phi_N]^T$, $\overline{\overline{h_c}}=[\overline{h_0}\cos\phi_0,\overline{h_1}\cos\phi_1,\ldots,\overline{h_N}\ cos\phi_N]^T$, and $\overline{\overline{h_s}}=[\overline{h_0}\sin\phi_0,\overline{h_1}\sin\phi_1,\ldots,\overline{h_N}\ sin\phi_N]^T$. Here $M_1(\beta)$, $M_2(\beta)$, $M_3(\beta)$, $M_4(\beta)$, $M_5(\beta)$, $M_6(\beta)$, $Y_c(\beta)$, $Y_s(\beta)$, $Y_{rc}(\beta)$, *and* $Y_{rs}(\beta)$ are diagonal matrices given in Appendix A. The matrices Q, H, R, U, T, and $\overline{\overline{W}}$ are defined by $Q=[Q_0,Q_1,\ldots,Q_N]$, $H=[H_0,H_1,\ldots,H_N]$, $R=[R_0,R_1,\ldots,R_N]$, $U=[U_0,U_1,\ldots,U_N]$, $T=[T_0,T_1,\ldots,T_N]$, and $\overline{\overline{W}}=[W_0,W_1,\ldots,W_N]$.

On the other hand, boundary conditions for the continuities of the electric field components at interfaces require

$$\mathbf{E_z^1}(\mathbf{x_1})=\mathbf{E_z^2}(\mathbf{x_1}) \tag{40}$$

$$\mathbf{E_z^2}(\mathbf{x_2})=\mathbf{E_z^3}(\mathbf{x_2}) \tag{41}$$

$$\mathbf{E_y^1}(\mathbf{x_1})=\mathbf{E_y^2}(\mathbf{x_1}) \tag{42}$$

$$\mathbf{E_y^2}(\mathbf{x_2})=\mathbf{E_y^3}(\mathbf{x_2}) \tag{43}$$

which, respectively, correspond to

$$HM_2(\beta)\overline{\overline{a}}=UM_4(\beta)\overline{\overline{f_s}} \tag{44}$$

$$UM_4(\beta)\left(Y_s(\beta)\overline{\overline{f_c}}-Y_c(\beta)\overline{\overline{f_s}}\right)=\overline{\overline{W}}M_2(\beta)\overline{\overline{d}} \tag{45}$$

$$M_1(\beta)^2\overline{\overline{b}}+HM_2(\beta)^3\overline{\overline{c}}+\overline{\overline{W}}HM_2(\beta)\overline{\overline{a}}=-RM_3(\beta)^2\overline{\overline{g_c}}-UM_3(\beta)^2\overline{\overline{h_s}}+\overline{\overline{W}}UM_4(\beta)\overline{\overline{f_s}} \tag{46}$$

$$\begin{aligned}RM_3(\beta)\left(Y_{rs}(\beta)\overline{\overline{g_c}}-Y_{rc}(\beta)\overline{\overline{g_s}}\right)+UM_4(\beta)^2\left(Y_c(\beta)\overline{\overline{h_c}}+Y_s(\beta)\overline{\overline{h_s}}+\overline{\overline{W}}UM_4(\beta)\left(Y_s(\beta)\overline{\overline{f_c}}-Y_c(\beta)\overline{\overline{f_s}}\right)\right)\\ =TM_5(\beta)\overline{\overline{m}}-\overline{\overline{W}}M_6(\beta)^2\overline{\overline{j}}-\overline{\overline{W}}RM_6(\beta)\overline{\overline{d}}\end{aligned} \tag{47}$$

where the column vector $\overline{\overline{j}}$ is equal to $[\overline{j_0},\overline{j_1},\ldots\ldots,\overline{j_N}]^T$. After mathematical manipulation, the equations corresponding to the boundary conditions given above reduce to a single matrix equation as follows:

$$\left[S_a(\beta)+S_b(\beta)\times S_x(\beta)\times S_y(\beta)\right]\times\overline{\overline{a}}=0 \tag{48}$$

where 0 represents a zero vector, and matrices $S_a(\beta)$, $S_b(\beta)$, $S_x(\beta)$, and $S_y(\beta)$ are functions of the propagation constant β. Since there exists a nontrivial solution for the arbitrary column vector $\overline{\overline{a}}$, the determinant of the matrix $[S_a(\beta)+S_b(\beta)\times S_x(\beta)\times S_y(\beta)]$ should be zero, from which the propagation constantβ can be solved using the Newton–Raphson root-shooting algorithm [30].

3. Efficiency and Accuracy of Numerical Results

To verify the performance in efficiency and accuracy of the proposed mode solver, we calculate the effective indices of the two rib-type waveguides having the cross section of Fig. 1. The two waveguides have the structural parameters as shown in Table 1. The operating wavelength

TABLE 1

Waveguide parameters of two rib waveguides under study

Parameters of Rib Waveguides #1 and # 2							
waveguide	n_1	n_2	n_3	d (μm)	h(μm)	w(μm)	t_{au}(μm)
#1	3.44	3.34	1	0.2	1.3	2	0
#2	3.44	3.34	1	0.2	1.3	2	0.01

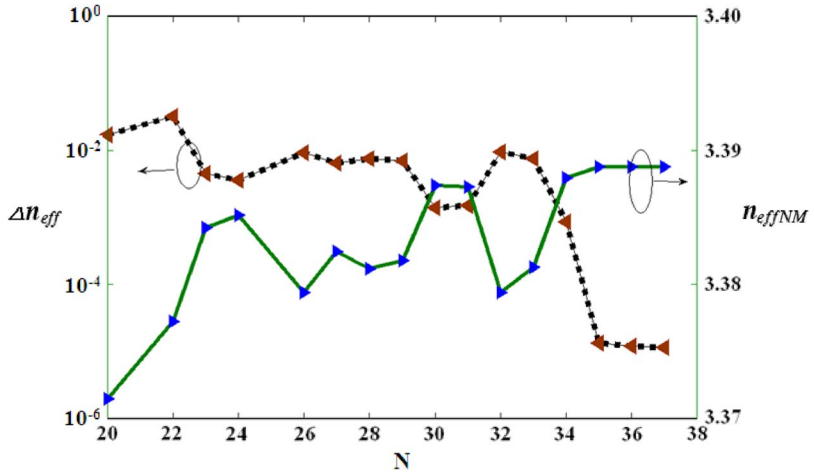

Fig. 2. Effective index of full-vectorial TE-mode n_{effNM} obtained by the proposed method and the relative errors Δn_{eff} of the mode index with respect to that obtained by BeamPROP as a function of N for waveguide #1.

$\lambda = 1.55$ μm is used in the study. For the example of waveguide #1, the indices $n_1 = 3.44$, $n_2 = 3.34$, and $n_3 = 1$, as well as $d = 0.2$ μm, $h = 1.3$ μm, and $w = 2$ μm are used. For the calculations, the windows sizes x_3 and y_4 are both set to be 6.4 μm. Generally, the numbers of the terms N in Fourier series expansion is required to be large enough to get accurate results. To calculate the effective index $n = (\beta/k_0)$ with our present method, we assigned an initial guess on n_{eff} that is an average value of the refractive indices in the guided layer and the substrate region. Here, we defined n_{effNM} and n_{effBP} as the effective indices obtained by the proposed method and BeamPROP, respectively, and calculated the relative errors $\Delta n_{eff} = |n_{effNM} - n_{effBP}|$ by increasing N value of the proposed method for waveguide #1. Fig. 2 shows the relative errors Δn_{eff} for the case of TE mode as a function of N. It is observed that the n_{effNM} approaches a steady value, i.e., 3.388787 as N increases up to 37. The CPU time spent for this calculation is 3.80 s. For comparison, values of n_{effBP} obtained by using the commercial software BeamPROP from Rsoft, Inc., are listed in Table 2, where we can observe convergence of n_{effBP} to 3.388782 with fine grid sizes of $\Delta x = 0.01$ μm, $\Delta y = 0.015$ μm, and $\Delta z = 0.1$ μm, with the CPU time of 50 s. Alternatively, the refractive index $n_{effCS} = 3.388690$ (3.388765) is obtained by COMSOL with element number 27586 (298573) at 79 (200) s CPU time. Obviously, the CPU time is much larger than that spent by the proposed method. The analysis for TM modal index of waveguide #1 was also calculated by the proposed method. Δn_{eff} of the TM mode versus N is shown in Fig. 3, where we can see that n_{effNM} becomes steady toward 3.387987 as N increases to 47 in comparison with n_{effBP} 3.387906 obtained by BeamPROP with grid size $\Delta x = 0.005$ μm, $\Delta y = 0.05$ μm, $\Delta z = 0.25$ μm, and $n_{effCS} = 3.387930$ (3.387938) obtained by COMSOL at CPU time 79 (200) s with element number 27586 (298573). The CPU time required by the proposed method in the calculation is 4.8 s, which is much less than that spent by using BeamPROP (see Table 3) or COMSOL. Figs. 4 and 5 show the contours of the major full-vectorial TE and TM modes at 10% interval levels of the maximum field, respectively. Note that these

TABLE 2

Mode indices of the full-vectorial TE mode calculated by the commercial software BeamPROP using different discretizations for waveguide #1. $x_3 = 6.4\ \mu$m and $y_4 = 6.4\ \mu$m are used

Grid size (μm)	n_{eff}	CPU (s)
$\triangle x$=$\triangle y$=0.05, $\triangle z$=0.5	3.388660	1.2
$\triangle x$=0.05, $\triangle y$=0.025, $\triangle z$=0.5	3.388780	2.7
$\triangle x$=$\triangle y$=0.025, $\triangle z$=0.5	3.388756	10
$\triangle x$=0.01, $\triangle y$=0.05, $\triangle z$=0.5	3.388598	17
$\triangle x$=0.01, $\triangle y$=0.025, $\triangle z$=0.5	3.388714	35
$\triangle x$=0.01, $\triangle y$=0.015, $\triangle z$=0.5	3.388774	44
$\triangle x$=0.01, $\triangle y$=0.025, $\triangle z$=0.25	3.388703	47
$\triangle x$=0.01, $\triangle y$=0.015, $\triangle z$=0.1	3.388782	50

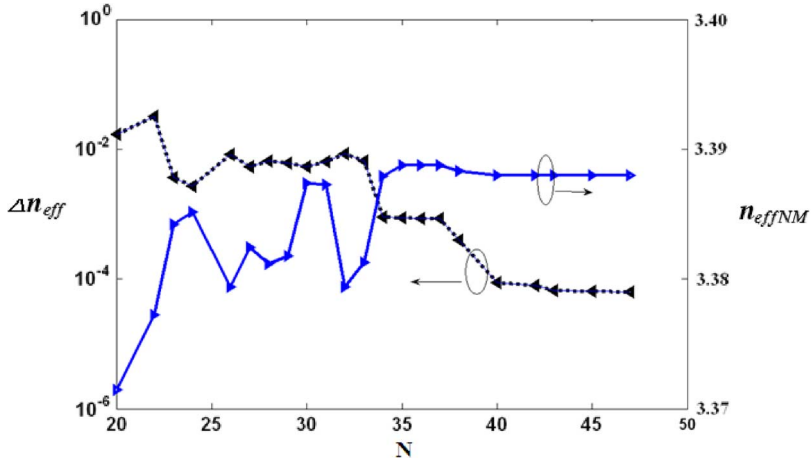

Fig. 3. Effective index of full-vectorial TM-mode n_{effNM} obtained by the proposed method and the relative errors Δn_{eff} of the modal index with respect to that obtained by BeamPROP as a function of N for waveguide #1.

two magnetic fields are concentrated in the regions of width of rib w that has verified clearly one period from $-x_3$ to x_3 assumed in the proposed method is large enough for numerical convergence. Figs. 6 and 7 are the contours of the minor full-vectorial TE and TM modes at 2% interval levels of the maximum field, respectively.

From the results above, we clearly find that the n_{effNM} obtained by the proposed method is in excellent agreement with an error of $10^{-5} \sim 10^{-6}$ with that obtained by BeamPROP and COMSOL, while the former is more time-efficient than the latter two. The requirement for larger CPU time by the FDM-based beam propagation method BeamPROP and by the FEM-based method COMSOL is due to the larger matrix dimension required in numerical calculation, while this disadvantage has been avoided in our approach. In the present method, CPU time spent is determined dominantly by the number of terms N taken for the calculation of (48) to reach a stable value. On the contrary, more CPU time is consumed in calculation of a large matrix dimension in BeamPROP and COMSOL for numerical convergence. The CPU time consumed in this case is based on a personal computer with 1.8 GHz CPU and 1 GB RAM. It can be seen from Table 2 that the calculated n_{effBP} by BeamPROP can not reach stable unless the grid sizes of Δx, Δy, and Δz are finely discretized and the n_{effCS} obtained by COMSOL as the element

TABLE 3

Mode indices of the full-vectorial TM mode calculated by the commercial software BeamPROP using different discretizations for waveguide #1. $x_3 = 6.4$ μm and $y_4 = 6.4$ μm are used

Grid size (μm)	n_{eff}	CPU (s)
Δx=Δy=0.05, Δz=0.5	3.387806	1.3
Δx=0.05, Δy=0.025, Δz=0.5	3.387616	2.8
Δx=Δy=0.025, Δz=0.5	3.387970	9
Δx=0.04, Δy=0.02, Δz=0.25	3.387850	18
Δx=Δy=0.02, Δz=0.25	3.387903	20
Δx=0.01, Δy=0.035, Δz=0.5	3.387911	29
Δx=0.005, Δy=0.05, Δz=0.25	3.387906	90

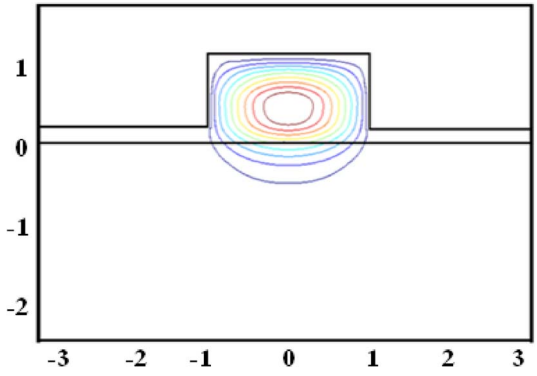

Fig. 4. Field distribution of the major full-vectorial TE mode H_y for waveguide #1.

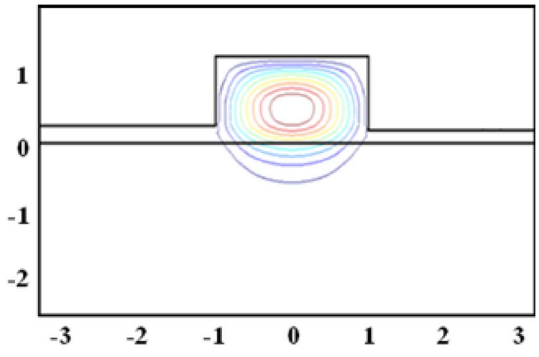

Fig. 5. Field distribution of the major full-vectorial TM mode H_x for waveguide #1.

number are finely taken. To further confirm the accuracy of the proposed scheme, Table 4 lists the numerical results including the mode index n_{eff} and the normalized propagation constant $(b = n_{eff}^2 - n_2^2/n_1^2 - n_2^2)$ obtained by the proposed method and by other available methods.

The second waveguide under study named waveguide #2 (surface plasmon waveguide) is a rib-type waveguide with structural parameters same as waveguide #1, except that an Au film with thickness $t_{au} = 10$ nm and the refractive index $n_{au} = 0.55 - j11.5$ [32]–[34] (at wavelength $\lambda = 1550$ nm) is deposited on top of the rib region. The converged refractive indices obtained by the proposed method in this case are $n_{effNM} = 3.388540 - j0.000285$ for full-vectorial TE

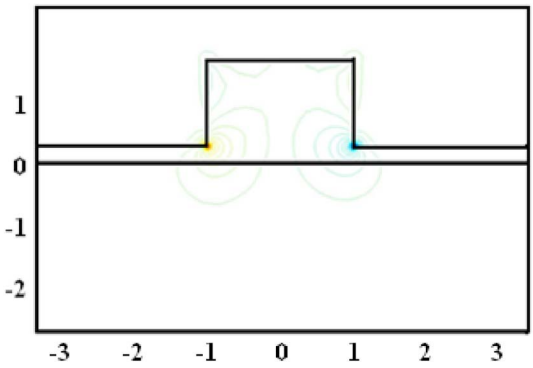

Fig. 6. Field distribution of the minor full-vectorial TE mode H_y for waveguide #1.

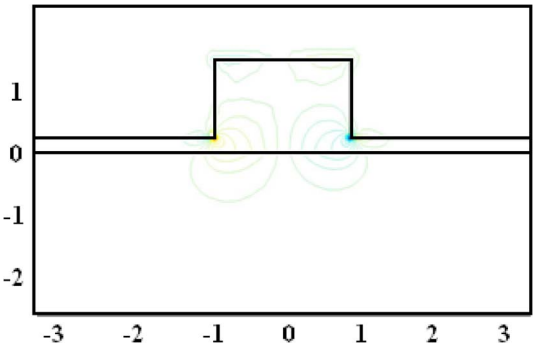

Fig. 7. Field distribution of the minor full-vectorial TM mode H_x for waveguide #1.

TABLE 4

Comparison of the modal index n_{eff} for waveguide #1 at $\lambda = 1.55$ μm obtained by the proposed method, BeamPROP, COMSOL, and other methods

i	Method	No. of Nodes	$\mathcal{K}_y$	b	$\mathcal{K}_x$	b
1	VM [22]	-----	3.388408	0.480396	3.387657	0.472890
2	SIM [31]	-----	3.388740	0.483715	3.387880	0.475119
3	SV-BPM [14]	-----	3.388711	0.483425	3.387924	0.475559
4	FV-FEM [10]	2795 elements	3.388699	0.483305	3.387865	0.474969
5	SFDM [25]	1280x1280	3.388658	0.482895	3.387868	0.474999
6	FV-FEM [9]	35x49—17x24 elements	3.388687	0.483185	3.387859	0.474909
7	BeamPROP	Δx=0.01, Δy=0.015, Δz=0.1 Δx=0.005, Δy=0.05, Δz=0.25	3.388782	0.484134	3.387906	0.475379
8	COMSOL	298573 elements	3.388765	0.483964	3.387938	0.475698
9	This work	N=37(for TE), N=47(for TM)	3.388787	0.484184	3.387987	0.476188

mode with $N = 62$ at 2.15 s CPU time and $n_{effNM} = 3.383983 - j0.000151$ for full-vectorial TM mode with $N = 69$ at 2.66 s CPU time, respectively.

For the purpose of comparison, we used the package, COMSOL, to model the same structure. In this simulation, we discretized the waveguide by taking high dense meshes at the metal

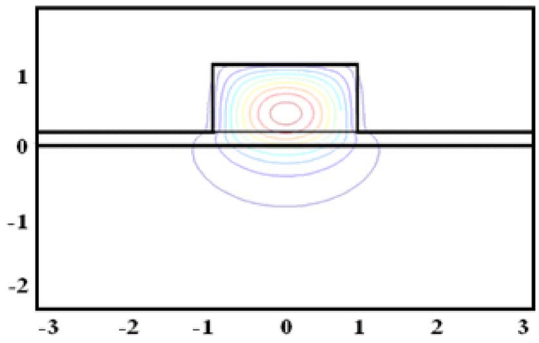

Fig. 8. Field distribution of the major full-vectorial TE mode H_y for waveguide #2.

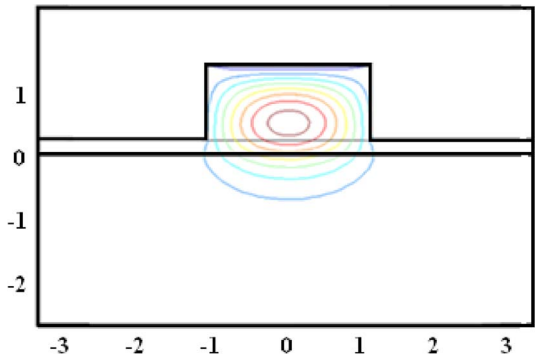

Fig. 9. Field distribution of the major full-vectorial TM mode H_x for waveguide #2.

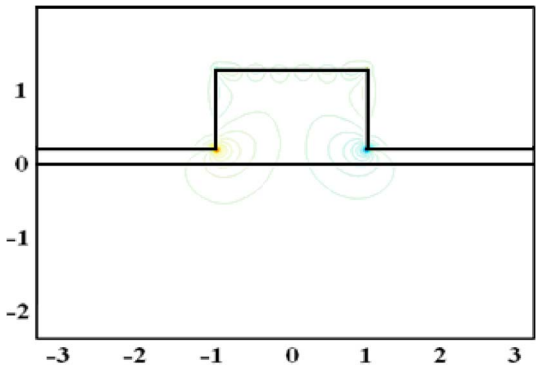

Fig. 10. Field distribution of the minor full-vectorial TE mode H_y for waveguide #2.

layer with $y = 1$ nm, while taking coarse discretizations for other regions. The effective indices $n_{effCS} = 3.388033 - j0.000058$ and $n_{effCS} = 3.3844082 - j0.000416$ were obtained by COMSOL with the element number of 22845 at 76 s CPU time for the full-vectorial TE and TM mode analyses, respectively. The CPU time spent in this case study was based on a personal computer with 8-core 2.13 GHz CPU. It was obvious that the effective indices of the proposed method are in good agreement with COMSOL, but the former seems to provide a less time-consuming means as compared to the latter. Figs. 8 and 9 are the contours of waveguide #2 for the major full-vectorial TE and TM magnetic field profiles at 10% interval levels of the maximum field, respectively. Figs. 10 and 11 sketch the contours of waveguide #2 for the minor full-vectorial TE and TM magnetic field profiles at 2% interval levels of the maximum field, respectively.

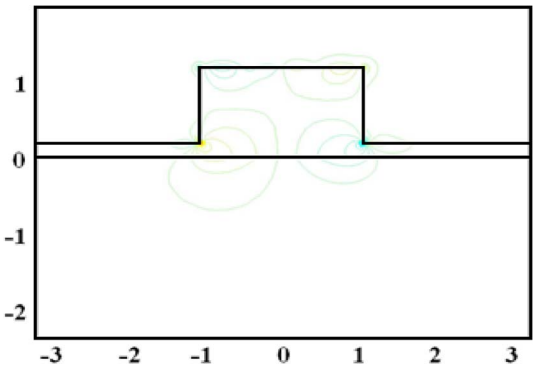

Fig. 11. Field distribution of the minor full-vectorial TM mode H_x for waveguide #2.

4. Conclusion

A highly efficient and accurate full-vectorial eigenmode solver is proposed and developed in this study. The proposed method is based on the Fourier cosine and sine series expansions of magnetic field distributions and refractive index profile that are substituted into the full-vectorial wave equation to subsequently result in a single matrix equation, i.e., (48) when boundary conditions are met. To demonstrate the accuracy and efficiency of the proposed method, two waveguides, including a traditional rib-type waveguide and a surface plasmon waveguide, were investigated in comparison with the widely-used commercial software programs BeamPROP and COMSOL. The calculated effective indices obtained by the proposed method compare well with those obtained by using BeamPROP and COMSOL. The numerical results show that the proposed method can be used for the full-vectorial modal analysis of dielectric optical waveguides with arbitrary structural parameters. Additionally, the proposed method appears to require comparatively less computation resource because a larger matrix is not required in the proposed scheme in contrast to FDM-based and FEM-based methods. The proposed algorithm significantly enhances computational efficiency and reduces memory storage required as compared with BeamPROP and COMSOL. Finally, we believe that the proposed method is also applicable to more complicated photonic device problems and will be studied in future work.

APPENDIX A

$$M_1(\beta) = \begin{bmatrix} \sqrt{\beta^2 - \alpha_0} & 0 & \cdot & \cdot & \cdot & 0 \\ 0 & \sqrt{\beta^2 - \alpha_1} & 0 & \cdot & \cdot & \cdot \\ 0 & 0 & \sqrt{\beta^2 - \alpha_2} & \cdot & \cdot & \cdot \\ \cdot & \cdot & 0 & \cdot & \cdot & \cdot \\ \cdot & \cdot & \cdot & \cdot & \cdot & 0 \\ 0 & \cdot & \cdot & \cdot & 0 & \sqrt{\beta^2 - \alpha_N} \end{bmatrix} \tag{A1}$$

$$M_2(\beta) = \begin{bmatrix} \sqrt{\beta^2 - \kappa_0} & 0 & \cdot & \cdot & \cdot & 0 \\ 0 & \sqrt{\beta^2 - \kappa_1} & 0 & \cdot & \cdot & \cdot \\ 0 & 0 & \sqrt{\beta^2 - \kappa_2} & \cdot & \cdot & \cdot \\ \cdot & \cdot & 0 & \cdot & \cdot & \cdot \\ \cdot & \cdot & \cdot & \cdot & \cdot & 0 \\ 0 & \cdot & \cdot & \cdot & 0 & \sqrt{\beta^2 - \kappa_N} \end{bmatrix} \tag{A2}$$

$$M_3(\beta) = \begin{bmatrix} \sqrt{\gamma_0 - \beta_2^2} & 0 & \cdot & \cdot & \cdot & 0 \\ 0 & \sqrt{\gamma_1 - \beta_2^2} & 0 & \cdot & \cdot & \cdot \\ 0 & 0 & \sqrt{\gamma_2 - \beta_2^2} & \cdot & \cdot & \cdot \\ \cdot & \cdot & 0 & \cdot & \cdot & \cdot \\ \cdot & \cdot & \cdot & \cdot & \cdot & 0 \\ 0 & \cdot & \cdot & \cdot & 0 & \sqrt{\gamma_N - \beta_2^2} \end{bmatrix} \tag{A3}$$

$$M_4(\beta) = \begin{bmatrix} \sqrt{\lambda_0 - \beta^2} & 0 & \cdot & \cdot & \cdot & 0 \\ 0 & \sqrt{\lambda_1 - \beta^2} & 0 & \cdot & \cdot & \cdot \\ 0 & 0 & \sqrt{\lambda_2 - \beta^2} & \cdot & \cdot & \cdot \\ \cdot & \cdot & 0 & \cdot & \cdot & \cdot \\ \cdot & \cdot & \cdot & \cdot & \cdot & 0 \\ 0 & \cdot & \cdot & \cdot & 0 & \sqrt{\lambda_N - \beta^2} \end{bmatrix} \tag{A4}$$

$$M_5(\beta) = \begin{bmatrix} \sqrt{\beta_2^2 - \sigma_0} & 0 & \cdot & \cdot & \cdot & 0 \\ 0 & \sqrt{\beta_2^2 - \sigma_1} & 0 & \cdot & \cdot & \cdot \\ 0 & 0 & \sqrt{\beta_2^2 - \sigma_2} & \cdot & \cdot & \cdot \\ \cdot & \cdot & 0 & \cdot & \cdot & \cdot \\ \cdot & \cdot & \cdot & \cdot & \cdot & 0 \\ 0 & \cdot & \cdot & \cdot & 0 & \sqrt{\beta_2^2 - \sigma_N} \end{bmatrix} \tag{A5}$$

$$M_6(\beta) = \begin{bmatrix} \sqrt{\beta_2^2 - \delta_0} & 0 & \cdot & \cdot & \cdot & 0 \\ 0 & \sqrt{\beta_2^2 - \delta_1} & 0 & \cdot & \cdot & \cdot \\ 0 & 0 & \sqrt{\beta_2^2 - \delta_2} & \cdot & \cdot & \cdot \\ \cdot & \cdot & 0 & \cdot & \cdot & \cdot \\ \cdot & \cdot & \cdot & \cdot & \cdot & 0 \\ 0 & \cdot & \cdot & \cdot & 0 & \sqrt{\beta_2^2 - \delta_N} \end{bmatrix} \tag{A6}$$

$$Y_c(\beta) = \begin{bmatrix} \cos\left(\sqrt{\lambda_0 - \beta^2}(x_2 - x_1)\right) & 0 & 0 & \cdot & 0 \\ 0 & \cos\left(\sqrt{\lambda_1 - \beta^2}(x_2 - x_1)\right) & 0 & \cdot & 0 \\ 0 & 0 & \cdot & \cdot & \cdot \\ \cdot & \cdot & \cdot & \cdot & \cdot \\ 0 & 0 & \cdot & 0 & \cos\left(\sqrt{\lambda_N - \beta^2}(x_2 - x_1)\right) \end{bmatrix} \tag{A7}$$

$$Y_s(\beta) = \begin{bmatrix} \sin\left(\sqrt{\lambda_0 - \beta^2}(x_2 - x_1)\right) & 0 & 0 & \cdot & 0 \\ 0 & \sin\left(\sqrt{\lambda_1 - \beta^2}(x_2 - x_1)\right) & 0 & \cdot & 0 \\ 0 & 0 & \cdot & \cdot & \cdot \\ \cdot & \cdot & \cdot & \cdot & \cdot \\ 0 & 0 & \cdot & 0 & \sin\left(\sqrt{\lambda_N - \beta^2}(x_2 - x_1)\right) \end{bmatrix} \tag{A8}$$

$$Y_{rc}(\beta) = \begin{bmatrix} \cos\left(\sqrt{\gamma_0 - \beta^2}(x_2 - x_1)\right) & 0 & 0 & \cdot & 0 \\ 0 & \cos\left(\sqrt{\gamma_1 - \beta^2}(x_2 - x_1)\right) & 0 & \cdot & 0 \\ 0 & 0 & \cdot & \cdot & \cdot \\ \cdot & \cdot & \cdot & \cdot & \cdot \\ 0 & 0 & \cdot & 0 & \cos\left(\sqrt{\gamma_N - \beta^2}(x_2 - x_1)\right) \end{bmatrix} \tag{A9}$$

$$Y_{rs}(\beta) = \begin{bmatrix} \sin\left(\sqrt{\gamma_0 - \beta^2}(x_2 - x_1)\right) & 0 & 0 & \cdot & 0 \\ 0 & \sin\left(\sqrt{\gamma_1 - \beta^2}(x_2 - x_1)\right) & 0 & \cdot & 0 \\ 0 & 0 & \cdot & \cdot & \cdot \\ \cdot & \cdot & \cdot & \cdot & \cdot \\ 0 & 0 & \cdot & 0 & \sin\left(\sqrt{\gamma_N - \beta^2}(x_2 - x_1)\right) \end{bmatrix} \tag{A10}$$

References

[1] P. Lusse, P. Stuwe, J. Schule, and H. G. Unger, "Analysis of vectorial mode fields in optical waveguides by a new finite difference method," *J. Lightw. Technol.*, vol. 12, no. 3, pp. 487–493, Mar. 1994.

[2] W. Huang, C. Xu, S.-T. Chu, and S. K. Chaudhuri, "The finite-difference vector beam propagation method: Analysis and assessment," *J. Lightw. Technol.*, vol. 10, no. 3, pp. 295–305, Mar. 1992.

[3] K. Jiang and W.-P. Huang, "Finite-difference-based mode-matching method for 3-D waveguide structures under semivectorial approximation," *J. Lightw. Technol.*, vol. 23, no. 12. pp. 4239–4248, Dec. 2005.

[4] G. G. Hadley, "High-accuracy finite equations for dielectric waveguide analysis I: Uniform regions and dielectric interfaces," *J. Lightw. Technol.*, vol. 20, no. 7, pp. 1210–1218, Jul. 2002.

[5] K. Bierwirth, N. Schulz, and F. Arndt, "Finite difference analysis of rectangular dielectric waveguide structures," *IEEE Trans. Microw. Theory Tech.*, vol. 34, no. 11, pp. 1104–1113, Nov. 1986.

[6] R. K. Lagu and R. V. Ramaswamy, "A variational finite-difference method for analyzing channel waveguides with arbitrary index profiles," *IEEE J. Quantum Electron.*, vol. 22, no. 6, pp. 968–976, Jun. 1986.

[7] Y.-C. Chiang, "Higher order finite-difference frequency domain analysis of 2-D photonic crystals with curved dielectric interfaces," *Opt. Exp.*, vol. 17, no. 5, pp. 3305–3315, Mar. 2009.

[8] K. Saitoh and M. Koshiba, "Full-vectorial imaginary-distance method based on a finite element scheme: Application to photonic crystal fibers," *IEEE J. Quantum Electron.*, vol. 38, no. 7, pp. 927–933, Jul. 2002.

[9] D. U. Li and H. C. Chang, "An efficient full-vectorial finite-element modal analysis of dielectric waveguides incorporating inhomogeneous elements across dielectric discontinuities," *IEEE J. Quantum Electron.*, vol. 36, no. 11, pp. 1251–1261, Nov. 2000.

[10] S. Selleri and J. Petracek, "Modal analysis of rib waveguide through finite element and mode matching methods," *Opt. Quantum Electron.*, vol. 33, no. 4/5, pp. 373–386, Apr. 2001

[11] M. Koshiba and Y. Tsuji, "Curvilinear hybrid edge/nodal element with triangular shape for guided-wave problems," *J. Lightw. Technol.*, vol. 18, no. 5, pp. 737–743, May 2000.

[12] Z. E. Abid, K. L. Johnson, and A. Gopinath, "Analysis of dielectric guides by vector transverse magnetic fields finite elements," *J. Lightw. Technol.*, vol. 11, no. 10, pp. 1545–1549, Oct. 1993.

[13] L. Wang and C. S. Hsiao, "A matrix method for studying TM modes of optical planar waveguides with arbitrary index profiles," *IEEE J. Quantum Electron.*, vol. 37, no. 12, pp. 1654–1660, Dec. 2001.

[14] P. L. Liu and B. J. Li, "Semi-vectorial beam propagation method for analyzing polarized modes of rib waveguides," *IEEE J. Quantum Electron.*, vol. 28, no. 4, pp. 778–782, Apr. 1992.

[15] C. H. Henry and B. H. Verbeek, "Solution of the scalar wave equation for arbitrary shaped dielectric waveguides by two-dimensional Fourier analysis," *J. Lightw. Technol.* vol. 7, no. 2, pp. 308–313, Feb. 1989.

[16] C. S. Hsiao, L. Wang, and Y. J. Cgiang, "An algorithm for beam propagation method in matrix form," *IEEE J. Quantum Electron.*, vol. 46, no. 3, pp. 332–339, Mar. 2010.

[17] C.-C. Huang, "Pseudospectral mode solver for analyzing nonlinear optical waveguides," *Opt. Exp.*, vol. 20, no. 12, pp. 13 014–13 029, Jun. 2012.

[18] P. J. Chiang, C. L. Wu, C. H. Teng, C. S. Yang, and H. C. Chang, "Full-vectorial optical waveguide mode solvers using multidomain pseudospectral frequency-domain (PSFD) formulations," *IEEE J. Quantum Electron.*, vol. 44, no. 1, pp. 56–66, Jan. 2008.

[19] B. Yang and J. S. Hesthaven, "A pseudospectral method for time-domain computation of electromagnetic scattering by bodies of revolution," *IEEE Trans. Antennas Propag.*, vol. 47, no. 1, pp. 132–141, Jan. 1999.

[20] C.-C. Huang, C.-C. Huang, and J.-Y. Yang, "A full-vectorial pseudospectral modal analysis of dielectric optical waveguides with stepped refractive index profiles," *IEEE J. Sel. Topics Quantum Electron.*, vol. 11, no. 2, pp. 457–465, Mar./Apr. 2005.

[21] E. E. Kriezis and A. G. Papagiannakis, "A three-dimensional full vectorial beam propagation method for z-dependent structures," *IEEE J. Quantum Electron.*, vol. 33, no. 5, pp. 883–890, May 1997.
[22] W. P. Huang and H. A. Haus, "A simple variational approach to optical rib waveguides," *J. Lightw. Technol.*, vol. 9, no. 1, pp. 56–61, Jan. 1991.
[23] T. Rozzi, G. Gerri, M. N. Husain, and L. Zappelli, "Variational analysis of the dielectric rib waveguide using the concept of 'transition function' and including edge singularities," *IEEE Trans. Microw. Theory Technol.*, vol. 39, no. 2, pp. 247–257, Feb. 1991.
[24] P. L. Liu and B. J. Li, "Semi-vectorial beam propagation method for analyzing polarized modes of rib waveguides," *IEEE J. Quantum Electron.*, vol. 28, no. 4, pp. 778–782, Apr. 1992.
[25] H. Noro and T. Nakayama, "A new approach to scalar and semivector mode analysis of optical waveguides," *J. Lightw. Technol.*, vol. 14, no. 6, pp. 1546–1556, Jun. 1996.
[26] S. A. Shakir, R. A. Motes and R. W. Berdine, "Efficient scalar beam propagation method," *IEEE J. Quantum Electron.*, vol. 47, no. 4, pp. 486–491, Apr. 2011.
[27] C. H. Henry, and Y. Shani, "Analysis of mode propagation in optical waveguide devices by Fourier expansion," *IEEE J. Quantum Electron.*, vol. 27, no. 3, pp. 523–530, Mar. 1991.
[28] D. Marcuse, "Solution of the vector wave equation for general dielectric waveguides by the Galerkin method," *IEEE J. Quantum Electron.*, vol. 28, no. 23, pp. 459–465, Feb. 1992.
[29] B. Young, "An improved formulation of an optimizing Rayleigh–Ritz technique for closed dielectric waveguide analysis," *IEEE Trans. Microw. Theory Technol.*, vol. 39, no. 11, pp. 1836–1846, Nov. 1991.
[30] V. N. Kublanovskaya, "On an application of Newton's method to the determination of eigenvalues of λ-matrices," *Soviet Math. Dokl.*, vol. 10, pp. 1240–1241, 1969.
[31] M. S. Stern, P. C. Kendall, and P. W. A. McIlory, "Analysis of the spectral index method for vector modes of rib waveguides," *Proc. Inst. Elect. Eng. J. Optoelectron.*, vol. 137, no. 1, pp. 21–26, Feb. 1990.
[32] R. Salvador, A. Martinez, C. Garcia-Meca, R. Ortuno, and J. Marti, "Analysis of hybrid dielectric plasmonic waveguides," *IEEE J. Sel. Topics Quantum Electron.*, vol. 14, no. 6, pp. 1496–1501, Nov./Dec. 2008.
[33] P. Flammer *et al.*, "Hybrid plasmon/dielectric waveguide for integrated silicon-on-insulator optical elements," *Opt. Exp.*, vol. 18, pp. 21 013–21 023, Sep. 2010.
[34] C.-C. Huang, Analysis of long-range surface plasmon polaritons in nonlinear plasmonic waveguides using pseudo-spectral method," *Opt. Exp.*, vol. 20, no. 175, pp. 18 665–18 678, Aug. 2012.